Investigation on the effects of Bragg reflection on harbor oscillations

Junliang Gao [a], Xiaozhou Ma [b *], Guohai Dong [b], Hongzhou Chen [c], Qian Liu [a], Jun Zang [d]

[a] School of Naval Architecture and Ocean Engineering, Jiangsu University of Science and Technology, Zhenjiang 212100, China

[b] The State Key Laboratory of Coastal and Offshore Engineering, Dalian University of Technology, Dalian 116024, China

[c] School of Civil Engineering and Architecture, Northeast Electric Power University, Jilin, 132012, China

[d] Centre for Infrastructure, Geotechnical and Water Engineering (IGWE), Department of Architecture and Civil Engineering, University of Bath, BA2 7AY, UK

Abstract:

Periodic undulating topographies (such as sandwaves and sandbars) are very common in coastal and estuarine areas. Normally incident water surface waves propagating from open sea to coastal areas may interact strongly with such topographies. The wave reflection by the periodic undulating topography can be significantly amplified when the surface wavelength is approximately twice the wavelength of the bottom undulations, which is often called as Bragg resonant reflection. Although the investigations on the hydrodynamic characteristics related to Bragg reflection of a region of undulating topography have been widely implemented, the effects of Bragg reflection on harbors have not yet been studied. Bragg resonant reflection can effectively reduce the incident waves. Meanwhile, however, it can also significantly hinder the wave radiation from the harbor entrance to the open sea. Whether Bragg reflection can be utilized as a potential measure to alleviate harbor oscillations is unknown.

In the present study, Bragg reflection and their interactions with the harbor are simulated using a fully nonlinear Boussinesq model, FUNWAVE 2.0. For the purpose, an elongated harbor with constant depth is considered, and a series of sinusoidal bars with various amplitudes and numbers are deployed outside the harbor. The incident waves considered in this paper include regular long waves and bichromatic short wave groups. It is revealed for the first time that for both kinds of

* Corresponding author: maxzh@dlut.edu.cn

incident waves, Bragg resonant reflection can significantly alleviate harbor resonance. The influences of the number and the amplitude of sinusoidal bars on the mitigation effect of harbor resonance and on the optimal wavelength of sinusoidal bars that can achieve the best mitigation effect are comprehensively investigated, and it is found that the former two factors have remarkable influences on the latter two parameters. The present research provides a new option for the mitigation of harbor oscillations via changing the bottom profile, which is feasible as long as the navigating depth is guaranteed.

Keywords:

Harbor oscillations; Harbor resonance; Bragg reflection; Sinusoidal bars; Regular long waves; Bichromatic short wave groups; FUNWAVE 2.0 model

1. Introduction

Harbor oscillations (also called *harbor resonance* or *seiches*) refer to the gathering and magnification of the incident wave energy inside bays or harbors, which can be triggered by atmospheric fluctuations, infragravity waves, tsunami waves, steady-state or transient wave groups, shear flows, or seisms (Bellotti, 2007; De Jong and Battjes, 2004; Fabrikant, 1995; Gao et al., 2017a; Gao et al., 2020; Kumar and Gulshan, 2017; Okihiro and Guza, 1996; Zheng et al., 2021). It may interrupt the operation of docks, create excessive movements of moored ships, cause unacceptable mooring forces, and even lead to the break of mooring lines (Gulshan et al., 2020; Kumar et al., 2016). The research progresses on harbor oscillations during the last three decades have been reviewed and summarized by Rabinovich (2009).

Harbor resonance phenomenon began to attract attention of coastal engineers from 1940s (Knapp and Vanoni, 1945), and the related scientific investigations started from the early 1950s (Vanoni and Carr, 1950). Most of existing studies focus on the stationary harbor resonance triggered by periodic oceanic waves propagating from the open sea, such as steady-state infragravity waves or steady-state short wave groups. Before the energy propagating from the external incident waves is balanced by energy dissipation generated by bottom friction, boundary absorption, and radiation from the entrance, the stationary resonance inside a bay or a harbor grows significantly (e.g., Gao et al. (2017b); Gao et al. (2019b); Kumar and Gulshan (2018); Losada et al. (2008); Wang et al.

(2014)). A small number of scholars have also implemented the investigations on the transient harbor oscillations, which are basically triggered by tsunami waves or transient wave groups (Endoh et al., 2018; Gao et al., 2021; Gao et al., 2019a; Gao et al., 2020).

Water surface waves scattered by the periodic undulating seabed have been widely investigated in the past four decades (e.g., Davies and Heathershaw (1984); Hsu et al. (2007); Liu et al. (2019a); Miles and Chamberlain (1998)). When investigating the issue of water surface waves propagating over a region of sinusoidal undulating topography, the most attractive phenomenon is the well-known Bragg resonant reflection of incident waves. When the wavelength of the periodic bottom undulations is approximately one half of the wavelength of the water surface waves, the overwhelming majority of the incoming waves could be reflected by the periodic undulating seabed, which would cause the significant decrease of the transmitted waves to the shoreline (Davies and Heathershaw, 1984; Liu et al., 2019b). The Bragg reflection phenomenon provide a possibility that periodic undulating seabeds at the offshore may decrease the wave energy propagating towards the coastline and protect the beach from energetic wave attack (Guo et al., 2021; Liu et al., 2015; Peng et al., 2019).

The investigations on the Bragg reflection phenomenon can be divided into two categories, that is, the theoretical study of Bragg reflection and its application research in the real coastal engineering. For the theoretical study, the sinusoidal undulating topography was most frequently considered, and various mathematical analysis methodologies were adopted to deduce the analytical solution for Bragg reflection, and the possible mechanism of the phenomenon were systematically revealed (e.g., Davies and Heathershaw (1984); Kar et al. (2020); Liu et al. (2019a); Miles and Chamberlain (1998)). In the aspect of engineering application, considering that Bragg reflection of periodic undulating seabed has significant wave prevention effect, in recent years, many scholars have carried out extensive studies on the influences of the section form, structural size and layout of the undulating seabed on Bragg reflection characteristics; the section forms of the undulating seabed considered mainly include rectangle, rectified cosine, trapezoid, triangle, semicircle, and so on (e.g., Li et al. (2020); Liu (2017); Liu et al. (2019b); Zeng et al. (2017)). Heretofore, the studies on Bragg reflection so far have been mostly confined to a region of periodic undulations set on flat or sloping seabeds, and both the seaward and leeward sides of the region of the periodic undulation were basically the simple horizontal bottom (Davies and Heathershaw, 1984; Kar et al., 2020; Kirby

and Anton, 1990; Liu, 2017; Miles and Chamberlain, 1998; Peng et al., 2019; Zeng et al., 2017; Zhang et al., 2012).

In coastal and estuarine areas, patches of periodic undulating topographies (such as sandwaves and sandbars) are frequently observed, with the wavelength ranging from a few meters to a few hundred meters (Boczar-Karakiewicz and Davidson-Arnott, 1987; Dolan and Dean, 1985; Elgar, 2003; Guazzelli et al., 1992; Zheng et al., 2016). Hence, the hydrodynamic interactions between the incident waves from the open sea, the periodic undulating topography and the harbor are very common in coastal and estuarine zones (e.g., for the Ponta da Madeira Harbor (Brazil) (Araújo et al., 2004), East London Harbor (South Africa) (Russell, 1982)), and Kesennuma Harbor (Japan) (Mogi, 1965)). However, to the best of the authors' knowledge, the coupling effects between the periodic undulation and the harbor subjected to water surface waves have not yet been investigated so far.

Although it has been widely acknowledged that Bragg reflection can significantly reflect the incident wave energy propagating from the offshore to the coastline when the patch of periodic undulation is set on flat or sloping seabeds, it is still unknow whether the periodic undulating topographies could notably weaken the strength of harbor oscillations if they are in front of the harbor entrance. The occurrence of Bragg resonant reflection can indeed significantly decrease the wave energy propagating into the harbor, which is beneficial to alleviate harbor oscillations. Meanwhile, however, when it occurs, the patch of periodic undulation could also significantly reflect the radiated waves from the harbor entrance back to the harbor, which would aggravate the intensity of harbor resonance. The specific influence of Bragg reflection on harbor resonance depends on the relative strength between the alleviating and the aggravating effects mentioned above.

Hence, the following four questions arise:

(1) Can the patch of periodic undulating topographies mitigate the strength of the harbor resonance induced directly by the incident regular long waves?

(2) If the answer to question (1) is yes, can the periodic undulating seabed further alleviate the harbor resonance triggered by the incident wave groups?

(3) If the answer to question (2) is yes, what a kind of spatial-scale relationship between the periodic undulating seabed and the incident waves should be satisfied? More specifically, there exist two possible spatial scale relationships: (i) the wavelength of undulating seabed is approximately equal

to half of the wavelength of the incident short waves, and (ii) the former is approximately equal to half of the wavelength of the incident wave groups. Which relationship should be satisfied?

(4) If both answers to questions (1) and (2) are yes, how the geometrical parameters of the periodic undulating topography (including the number and the amplitude) affect the mitigation effect for harbor resonance and the optimal wavelength of the undulating topography that can achieve the best mitigation effect?

To answer these questions, in this article, the interactions between a region of periodic undulating seabed, a harbor and incident steady-state surface waves will be systematically investigated for the first time. The incident steady-state waves considered in the present study include regular long waves and bichromatic short wave groups. The periodic undulating seabed is represented by sinusoidal bars which have been frequently adopted in the study of Bragg reflection (e.g., Davies and Heathershaw (1984); Liu et al. (2019a); Liu et al. (2019b); Miles and Chamberlain (1998)). The generation and propagation of the incident steady-state waves and their interactions with both the sinusoidal bars and the harbor are performed by using a Boussinesq-type numerical model. For simplification, the crest/trough lines of the sinusoidal bars are set to be parallel to and outside the harbor entrance. The harbor is assumed to be long and narrow; the free-surface displacement inside them essentially becomes one-dimensional. Except over the region of periodic undulating seabed, the water depth inside and outside the harbor is set to a constant.

The influences of the sinusoidal bars on the harbor resonance induced by the regular long waves are first examined and the capacity of Bragg reflection to mitigate the strength of harbor resonance is revealed for the first time in this study. Further, the effects of the number and the amplitude of the sinusoidal bars are examined on the mitigation effect for harbor resonance and on the optimal wavelength of the sinusoidal bars that can achieve the best mitigation effect. The lowest four resonant modes of the harbor are considered to reveal the sensitivity of the research findings to the resonant mode. Then, both the capability of Bragg reflection to restrain the harbor resonance induced by the bichromatic short wave groups and what a kind of spatial-scale relationship should be satisfied are proved and determined by setting two sets of sinusoidal bars with different wavelength ranges. How the geometric parameters of the sinusoidal bars affect the strength of harbor resonance and the optimal topographic wavelength is also discussed. However, different from regular long waves, the above discussions are only limited to the lowest resonant mode of the harbor

when the bichromatic short wave groups are considered.

The remainder of the paper is organized as follows: Section 2 briefly describes the numerical model, and its abilities to reproduce various hydrodynamic phenomena related to Bragg reflection and harbor resonance are verified by three sets of physical experiments. Section 3 introduces the parameters of the incident waves and illustrates the numerical wave tank as well. Section 4 describes the simulation results along with detailed explanations. Conclusions are finally drawn in Section 5.

2. Numerical model

2.1. Numerical model description

In the article, all numerical experiments are carried out by using the fully nonlinear Boussinesq-type numerical model, FUNWAVE 2.0, which has been widely used to simulate the wave transformation from the offshore area to the coastline in the community of coastal engineering. It was developed at University of Delaware by Kirby et al. (2003). This numerical model adopts a finite difference scheme to solve the fully nonlinear Boussinesq equations of Wei et al. (1995), and blends a moving reference level as performed in Kennedy et al. (2001).

The governing equations in FUNWAVE 2.0 are expressed as

$$h_t + \nabla \cdot \mathbf{M} = 0, \tag{1}$$

and

$$\mathbf{u}_{at} + (\mathbf{u}_a \cdot \nabla)\mathbf{u}_a + g\nabla h + \mathbf{V}_1 + \mathbf{V}_2 = 0, \tag{2}$$

where

$$\mathbf{M} = (h+h)\mathbf{u}_a + (h+h)\left[\frac{z_a^2}{2} - \frac{1}{6}(h^2 - hh + h^2)\right]\nabla(\nabla \cdot \mathbf{u}_a) + (h+h)\left[z_a + \frac{1}{2}(h-h)\right]\nabla(\nabla \cdot h\mathbf{u}_a), \tag{3}$$

$$\mathbf{V}_1 = \frac{z_a^2}{2}\nabla(\nabla \cdot \mathbf{u}_{at}) + z_a\nabla(\nabla \cdot h\mathbf{u}_{at}) - \nabla\left[\frac{1}{2}h^2\nabla \cdot \mathbf{u}_{at} + h\nabla \cdot (h\mathbf{u}_{at})\right], \tag{4}$$

$$\mathbf{V}_2 = \nabla\left[(z_a - h)(\mathbf{u}_a \cdot \nabla)(\nabla \cdot (h\mathbf{u}_a)) + \frac{1}{2}(z_a^2 - h^2)(\mathbf{u}_a \cdot \nabla)(\nabla \cdot \mathbf{u}_a)\right] + \frac{1}{2}\nabla\left[(\nabla \cdot (h\mathbf{u}_a) + h\nabla \cdot \mathbf{u}_a)^2\right]. \tag{5}$$

In these equations, η, h, t, and g denote the free wave surface, the water depth, the time, and the gravitational acceleration, respectively. $\mathbf{u}_\alpha$ denotes the vector of the horizontal velocity at a reference

elevation $z_\alpha=\alpha h$ with $\alpha=-0.531$. The subscript t denotes the first-order time partial derivative of the corresponding variable. $\nabla=(\partial/\partial x, \partial/\partial y)$ denotes the horizontal gradient vector.

The wave-making methodology of Chawla and Kirby (2000) is used to generate regular or irregular waves. At the boundaries of the numerical wave tank, sponge layers are arranged to dissipate outgoing waves with different frequencies and directions effectively. With the great improvement in both nonlinearity and dispersion, the numerical model can model the propagation and transformation of the water waves from intermediate depth to coastline accurately and robustly (Bruno et al., 2009; Gao et al., 2018; Kirby et al., 2003).

2.2. Numerical model verification by physical experiment

To the best of our knowledge, heretofore, the experimental data for the coupling interaction between Bragg reflection and harbor resonance have not yet been reported. Hence, the capability of the present model to reproduce Bragg reflection of water surface waves and to reproduce harbor resonance will be separately validated by using existing laboratory experiments in the following. The validation for Bragg reflection is shown in subsection 2.2.1. The verifications for harbor resonance are presented in subsections 2.2.2 and 2.2.3 where the linear harbor resonance and the nonlinear harbor resonance are respectively reproduced.

2.2.1. Bragg reflection over sinusoidal bars

To examine the ability of FUNWAVE 2.0 in simulating Bragg reflection excited by water surface waves, this model is used to reproduce the laboratory experiments of Davies and Heathershaw (1984). The experiments were carried out in a glass-walled wave tank with the dimensions of 45.72 m × 0.91 m × 0.91 m. A patch of sinusoidal bars with the wavelength of S= 1.0 m was built into a false bottom in the tank. Based on their experiments, the setup of the numerical wave tank used is shown in Fig. 1, where D and N respectively denote the amplitude and the number of sinusoidal bars. $L_s=NS$ denotes the total spatial length of the patch of bars whose left and right boundaries are respectively marked out by the symbols "B_L" and "B_R". The length of the numerical wave tank is set to 42 m, slightly shorter than that of the physical tank. The grid size is 0.02 m, and sponge layers with the width of 6 m are deployed at both sides to absorb the reflected and the transmitted waves. Two wave gauges (i.e., G_1 and G_2) are placed in front of the bars to calculate the

reflection coefficient, C_r, according to the two-point method proposed by Goda and Suzuki (1976). Two physical experiments with different bar numbers and water depths are reproduced here, and their specific parameters are listed in Table 1. In Tests 1 and 2, the numbers of bars are 4 and 10, respectively; the water depths are 0.156 m and 0.313 m, respectively. The amplitude of bars is D=0.05 m in both tests.

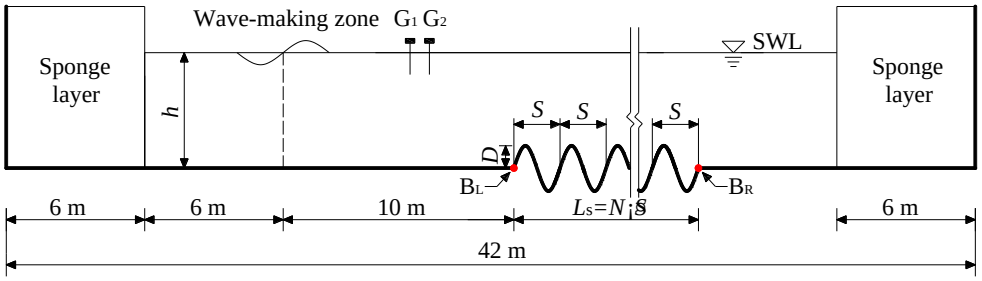

Fig. 1. Front view of the numerical wave flume for reproducing the experiments of Davies and Heathershaw (1984).

Table 1. Geometric parameters of sinusoidal bars and water depths for two experiments in Davies and Heathershaw (1984).

Test	S (m)	D (m)	N	h_0 (m)	D/h_0
01	1.0	0.05	4	0.156	0.321
02	1.0	0.05	10	0.313	0.160

For each test, a series of cases with various wavelengths of the incident regular waves are simulated, and all cases are run for 80 wave periods. The time series of the free-surface elevations for the last 30 waves recorded by G_1 and G_2 are selected for analyses. Fig. 2 presents the variations of both the measured and the simulated reflection coefficients with respect to the dimensionless parameter $2S/L$, where L denotes the wavelength of the incident waves. The analytical solutions of Liu et al. (2019a) that is based on the modified mild-slope equation and the numerical results of the Boussinesq model from Hsu et al. (2007) are also plotted here for comparison. It is observed that the predictions of FUNWAVE 2.0 agree reasonably with the experimental results for both tests and are also very close to both the analytical solutions of Liu et al. (2019a) and the numerical results of Hsu et al. (2007) overall. This indicates that the Bragg reflection of the sinusoidal bars can be

accurately simulated by the present model.

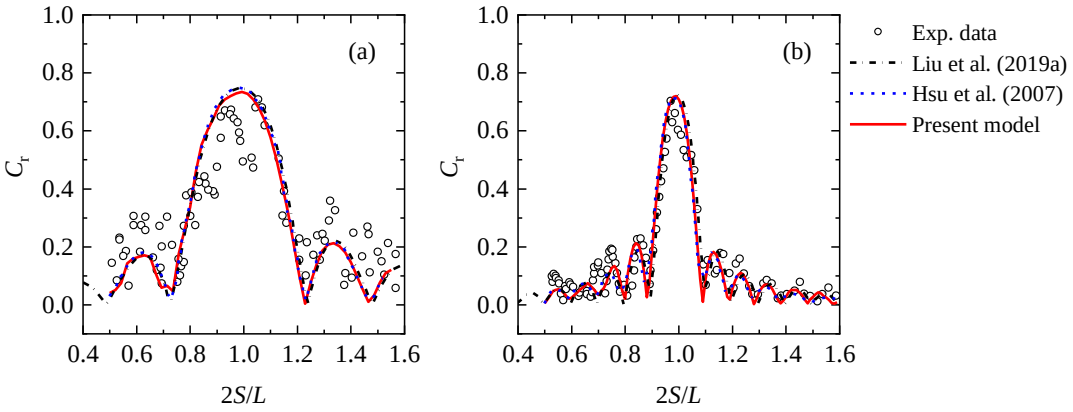

Fig. 2. Comparisons between simulated reflection coefficients and experimental data for the sinusoidal bars in (a) Test 01 and (b) Test 02. *L* in this figure denotes the wavelength of the incident waves.

2.2.2. Linear harbor oscillations

In this subsection, the classical resonance problem in an elongated harbor is considered. The ratio of the incident wave amplitude and the water depth is quite small so that the harbor response is linear. The purpose of performing the test for the linear harbor resonance is to validate the ability of the model for accurately estimating the resonant frequencies and the resonant wave amplitudes for various modes.

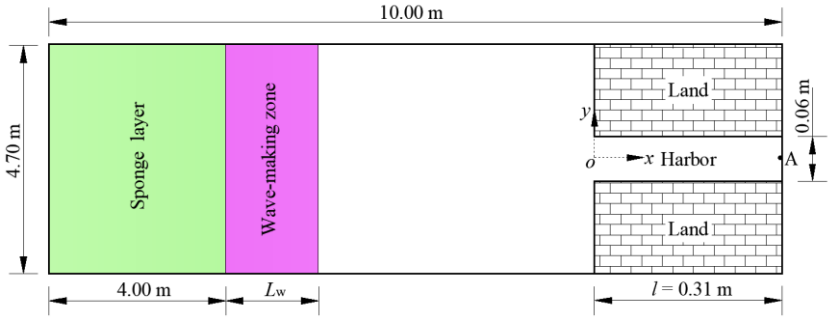

Fig. 3. Schematic top view of the numerical wave flume for reproducing the experiments of Ippen and Goda (1963) and Lee (1971). L_w and l denote the width of the wave-making zone and the length of the harbor, respectively.

Ippen and Goda (1963) and Lee (1971) implemented a series of physical experiments to study

the response of an elongated harbor with the length of l=0.31 m and the width of 0.06 m to the incident regular waves with various wavelengths. The water depth was set to h=0.26 m. The measured data were recorded at the center of the backwall of the harbor. The numerical wave tank adopted is shown in Fig. 3. The dimensions of the tank are 10.00 m × 4.70 m. A sponge layer with the width of 4.00 m is deployed at the left boundary to absorb the reflected and radiated waves. In the x-direction, except in the sponge layer at the left boundary, the grid size Δx is a constant of 0.010 m both inside and outside the harbor; Δx in the sponge layer gradually increase from 0.010 m to 0.179 m to save the computational time. In the y-direction, the grid size Δy gradually increases from 0.006 m inside the harbor to 0.191 m outside the harbor. The width of the wave-making zone, L_w, is always set to be one wavelength of the incident waves. A wave gauge is deployed at the center of the backwall of the harbor (i.e., the point A). Based on the experimental data, the incident wave amplitude, a, is set to 0.003 m, and hence it can be seen that the wave nonlinearity is quite small (a/h=0.01).

Fig. 4 presents the comparison of the present simulation results and experimental data. The linear analytical solution of Mei (1983) is also plotted here. For the lowest two resonant modes, their resonant frequencies predicted by the present model are in quite agreement with both the linear analytical solution and the experimental data. As for the resonant wave amplitudes, the simulated results also coincide well with the experimental measurements for both resonant modes overall. This proves that the FUNWAVE 2.0 model can predict the resonant frequencies and the resonant wave amplitudes accurately for various modes.

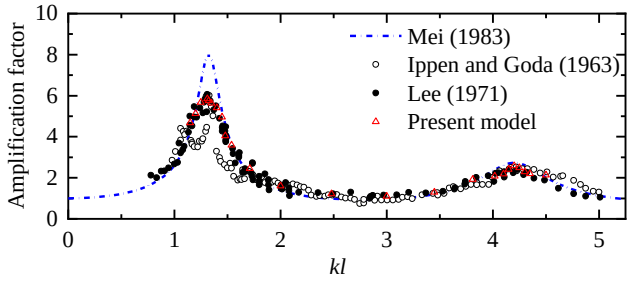

Fig. 4. Amplification factor curve at the center of the backwall (the point A) for the elongated rectangular harbor presented in Fig. 3. k (=$2\pi/L$) in this figure denote the wave number of the incident waves.

2.2.3. Nonlinear harbor oscillations

Rogers and Mei (1978) carried out experiments in a physical wave tank to investigate the nonlinear oscillations of three bays (Bay 1, Bay 2, and Bay 3) whose lengths are l=0.37 m, 1.27 m, and 2.18 m, respectively. The widths of the three bays are uniform and equal to b=0.10 m, and the water depth is h=0.15 m. The regular waves with a period of 1.545 s (correspondingly, with the wavelength of 1.79 m) were produced by the wavemaker.

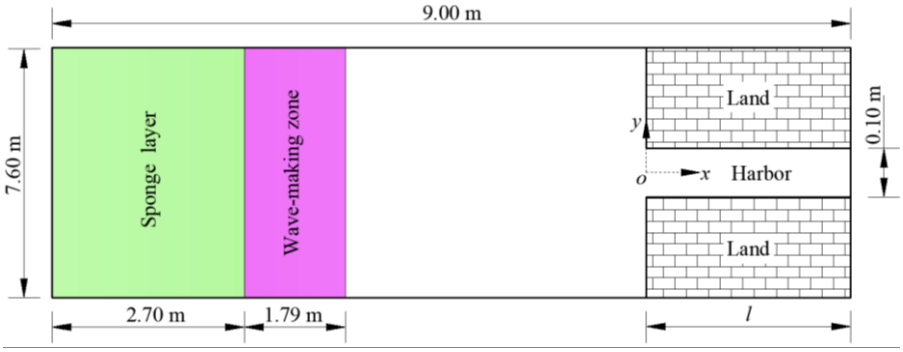

Fig. 5. Schematic top view of the numerical wave flume for reproducing the experiments of Rogers and Mei (1978).

The numerical wave tank utilized for simulations is presented in Fig. 5. The dimensions of the tank are 9.00 m × 7.60 m. A sponge layer with the width of 2.70 m is arranged at the left boundary. The incident regular waves with the wave height H/h=0.03 are generated in the internal wavemaker to reproduce parts of the laboratory experiments. The grid size Δx is a constant of 0.01 m both inside and outside the harbor except in the sponge layer where Δx gradually increase from 0.01 m to 0.10 m. The grid size Δy gradually increases from 0.01 m inside the harbor to 0.07 m outside the harbor.

Fig. 6 shows the comparisons of the simulated results of the first three super harmonics with the experimental data for the three bays. It can be easily seen that, for all the three bays and for all three super harmonics, the numerical results are in good coincidence with the measured data overall. This shows that the numerical model can well simulate the nonlinear energy transfer between various harmonic components during harbor resonance.

It should be noted that for the nonlinear harbor resonance induced by the bichromatic short wave groups (it will be elaborated in Section 3), its generation mechanism is essentially the transfer of wave energy from the short wave components to the 2nd-order difference-frequency (sub-harmonic) component. The good performance of the present model in modeling nonlinear wave

energy transfer between various harmonic components during harbor resonance guarantees that the nonlinear harbor resonance excited by the bichromatic wave groups can also be accurately simulated by the present model.

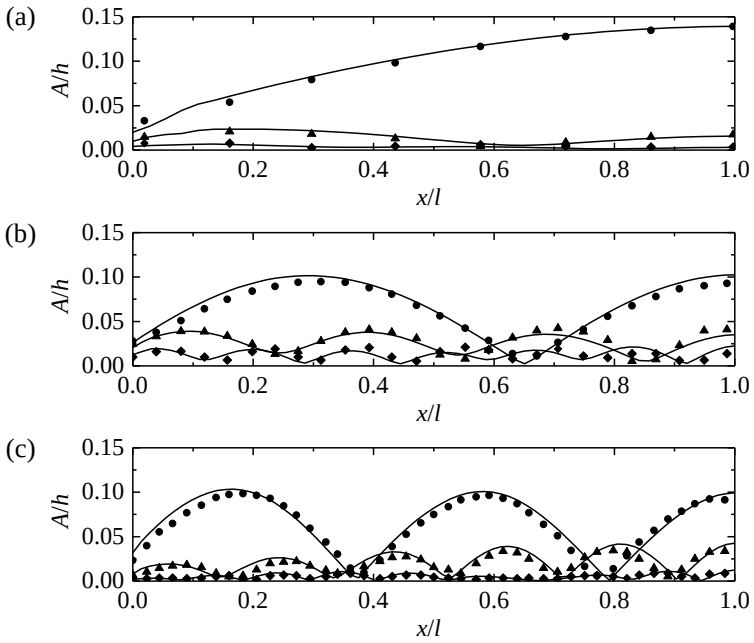

Fig. 6. Comparisons between the experimental data of Rogers and Mei (1978) and simulated results with for (a) Bay 1, (b) Bay 2, and (c) Bay 3. ●, fundamental harmonic; ▲, second harmonic; ◆, third harmonic; —, simulated results.

3. Numerical experimental setup

3.1. Incident wave parameters

The harbor oscillations triggered by two kinds of incident steady-state waves (i.e., regular long waves and bichromatic short wave groups) are investigated in the present study. Hence, the parameters for these two kinds of incident waves are separately presented in subsections 3.1.1 and 3.1.2.

3.1.1. Incident regular long waves

In this article, an elongated rectangular harbor with the length of l=20 m, the width of b=2 m and a constant water depth of h_0=1 m is considered. Based on the linear analytical solution of Mei

(1983), the amplification factor curve at the center of the backwall is calculated and presented in Fig. 7. It is seen that the lowest five resonant frequencies for the harbor are 0.035 Hz, 0.108 Hz, 0.180 Hz, 0.249 Hz, and 0.313 Hz. Because the lowest four resonant modes are investigated for the harbor resonance excited directly by regular long waves, the frequencies of the incident regular waves are set equal to the lowest four resonant frequencies. The incident wave height is H=0.02 m for all cases. Specific wave parameters for the harbor resonance triggered directly by the incident regular long waves are listed in Table 2. T_i and L_i in the table refer to the period and the wavelength of the incident waves with the frequency f_i (i=1, 2, 3 and 4), and L_i is determined according to the linear dispersion relation.

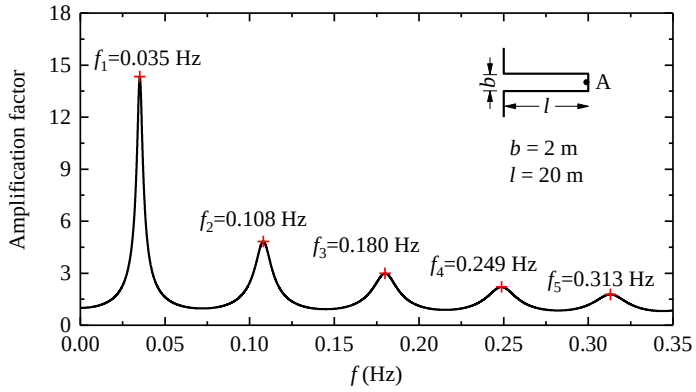

Fig. 7. Amplification factor curve at the center of the backwall (the point A) predicted by the analytical solution of Mei (1983) for the harbor shown in this figure. f_i denotes the resonant frequency of the i^{th} mode (Mode i).

Table 2. Specific parameters of both the incident waves and the sinusoidal bars for the harbor resonance triggered directly by regular long waves. T_i and L_i denotes the period and the wavelength of the incident waves with the frequency f_i (i=1, 2, 3 and 4), and the latter (L_i) is calculated based on the linear dispersion relation. H denotes the incident wave height.

Mode i	Parameters of incident waves				Parameters of sinusoidal bars		
	f_i (Hz)	T_i (s)	L_i (m)	H (m)	N	D (m)	$2S/L_i$
1	0.035	28.57	89.41	0.02	0, 2, 4, 6, 8	0.1, 0.2, 0.3 ,0.4	0.5~1.5
2	0.108	9.26	28.77	0.02	0, 2, 4, 6, 8	0.1, 0.2, 0.3 ,0.4	0.5~1.5
3	0.180	5.56	17.02	0.02	0, 2, 4, 6, 8	0.1, 0.2, 0.3 ,0.4	0.5~1.5
4	0.249	4.02	12.05	0.02	0, 2, 4, 6, 8	0.1, 0.2, 0.3 ,0.4	0.5~1.5

3.1.2. Incident bichromatic short wave groups

For the harbor resonance triggered by incident bichromatic short wave groups, only the first (i.e., the lowest) resonant mode of the harbor is investigated. To ensure the occurrence of the first resonant mode, the frequencies of the bichromatic short wave are set to F_1=0.265 Hz and F_2=0.300 Hz so that the beat frequency $\Delta f=|F_1-F_2|$=0.035 Hz corresponds to the resonant frequency of the first mode. Based on the linear dispersion relation, the wavelength of the free long waves generated near the harbor entrance and over the patch of sinusoidal bars outside the harbor (if any) is also equal to L_1=89.41 m. We define $\zeta=(\zeta_1+\zeta_2)/2$ as the wavelength of the incident short waves. ζ_i (i=1 and 2) denotes the wavelength of the short wave component with the frequency F_i and is determined based on the linear dispersion relation as well. The amplitudes for the bichromatic short waves are set to $a_1=a_2$=0.05 m. Specific wave parameters for the harbor resonance excited by the bichromatic short wave groups are listed in Table 3.

Table 3. Specific parameters of both the incident waves and the sinusoidal bars for the harbor resonance excited by bichromatic short wave groups.

Mode	Parameters of incident waves							Parameters of sinusoidal bars			
	F_1 (Hz)	F_2 (Hz)	Δf (Hz)	L_1 (m)	ζ (m)	a_1 (m)	a_2 (m)	Type	N	D (m)	$2S/L_1$ or $2S/\zeta$
1	0.265	0.300	0.035	89.41	10.53	0.05	0.05	Long-bar	0, 2, 4, 6, 8	0.1, 0.2, 0.3 ,0.4	0.5~1.5
								Short-bar	0, 2, 4, 6, 8	0.1, 0.2, 0.3 ,0.4	0.5~1.5

3.2. Numerical wave tank

The numerical wave tank and the definition of the coordinate system for the current study are shown in Fig. 8. As mentioned above, the harbor has the dimensions of 20 m × 2 m. Because the lowest four resonant modes are considered in the current study and the incident regular wavelengths for different resonant modes vary over a wide range (see Table 2), the length of the computational domain outside the harbor is designed according to the incident wavelength for each mode and is equal to $9.5L_i$. While the width of the wave tank for all the four resonant modes is always set to 20 m. In the x- and the y-directions, two uniform grid sizes, Δx=0.25 m and Δy=0.20 m, are utilized in the whole computational domain. For each resonant modes, the total time of 60 wave periods is simulated, and the time step of Δt=0.03 s is adopted. Twenty-one wave gauges (G_1-G_{21}) are deployed

equidistantly along the central line of the harbor, and the distance between adjacent gauges is 1.0 m. Gauges G_1 and G_{21} are placed at the backwall and the entrance of the harbor, respectively.

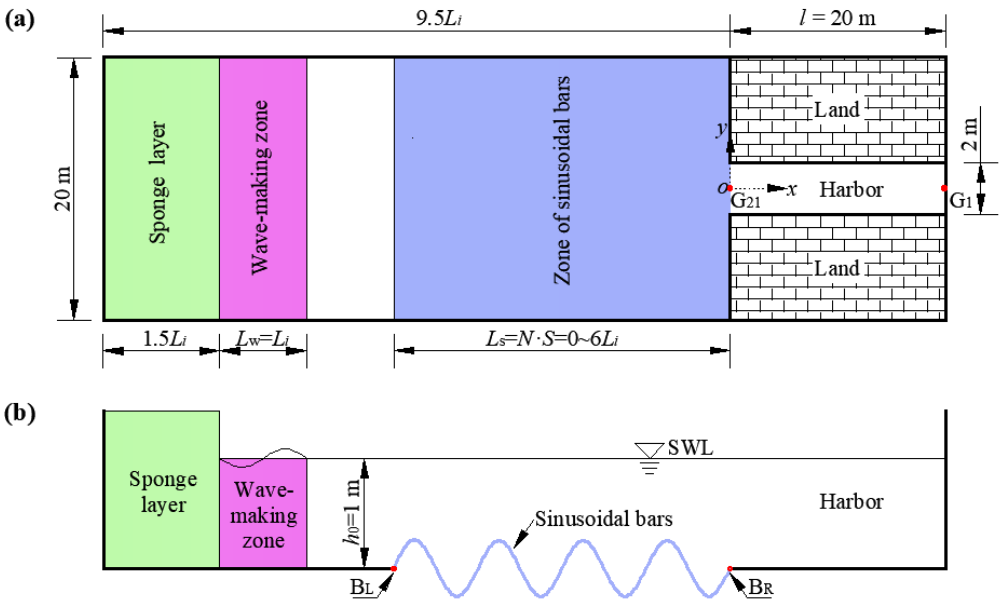

Fig. 8. Definition sketch of the numerical wave flume and the definition of the coordinate system for the present investigations: (a) the top view of the wave flume, (b) the front view of the cross section with y=0 (taking the sinusoidal bars with N=4 as an example).

A sponge layer with the width of 1.5L_i is arranged at the left boundary to dissipate the reflected and the radiated waves. The width of the wave-making zone always is equal to one wavelength of the incident waves. To investigate the influences of Bragg reflection on harbor resonance, a patch of sinusoidal bars with various geometric parameters are deployed outside the harbor entrance, and the crest/trough lines of sinusoidal bars are parallel to the harbor entrance. Meanwhile, the right boundary of the former, B_R, is always collinear with the latter.

The geometric parameters of the bars for the condition of incident regular long waves are also shown in Table 2. For each resonant mode, five bar numbers (i.e., N=0, 2, 4, 6, and 8) and four bar amplitudes (i.e., D=0.1 m, 0.2 m, 0.3 m, and 0.4 m) are considered. For all the four resonant modes, the normalized wavelengths of the bars, 2S/L_i, always vary at the range of 0.5~1.5. Hence, the spatial range for the patch of bars, L_s=NS, shown in Fig. 8 varies from 0 to 6L_i. The water depth in the whole computational domain is set to a constant of h_0=1.0 m except over the patch of bars, thus can be expressed as

$$h=\begin{cases} h_0 & \text{when } 0<x<l,\ |y|\le b/2 \\ h_0-D\sin(2\pi x/S) & \text{when } -L_s<x\le 0,\ |y|\le 10\text{ m} \\ h_0 & \text{when } -9.5L_i\le x\le -L_s,\ |y|\le 10\text{ m} \end{cases} \tag{6}$$

For the harbor oscillations excited by the bichromatic short wave groups, only the first resonant mode of the harbor is considered. To answer the questions (2) and (3) raised in the Introduction, two types (i.e., long-bar type and short-bar type) of sinusoidal bars are taken into considerations here (see Table 3). For the long-bar type topography, all setups about the wave tank are identical to those adopted in simulating the first resonant mode induced by regular long waves, except that the bichromatic short wave groups are simulated here. While for the short-bar type topography, the setups about the wave tank are identical to those for the long-bar type topography, except that the spatial scale of the short bars is designed according to the wavelength of the incident short waves, ζ, rather than to the wavelength of the free long waves, L_1.

It should be noted here that N=0 means no sinusoidal bar existing outside the harbor. In other words, only the pure harbor resonance process is simulated. The purposes of considering the cases with N=0 lies in constructing the comparative group for the cases with N>0.

4. Results and discussion

The time series of the wave surfaces and the spatial distribution of the wave amplitudes inside the harbor subjected to both the regular long waves and the bichromatic short wave groups are first analyzed in subsection 4.1 by using various data analysis techniques. Based on the analysis results in subsection 4.1, the effects of Bragg reflection on the harbor oscillations excited by the incident regular long waves are discussed in subsection 4.2. Finally, all the analysis results related to the influences of Bragg reflection on the harbor resonance triggered by the incident bichromatic short wave groups are presented in subsection 4.3.

4.1. Time series of free surface and spatial distributions of wave amplitudes

4.1.1. Incident regular long waves

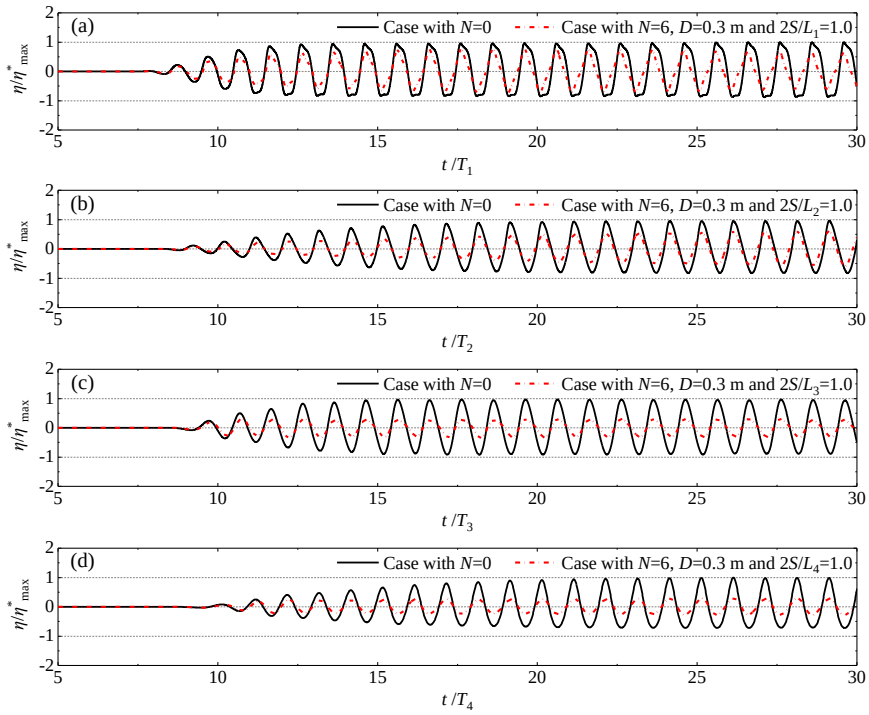

Fig. 9. Time series of the free surfaces at gauge G_1 for the no-bar topography (i.e., N=0) and for the sinusoidal bars with N=6, D/h_0=0.3 and $2S/L_i$=1.0 (i=1, 2, 3 and 4). (a)–(d) correspond to Modes 1–4, respectively. η denotes the free-surface elevation. η^*_{max} denotes the maximum free-surface elevation during the whole simulation for the no-bar topography.

Fig. 9 presents the comparisons between the time series of the free surfaces at G_1 for the no-bar topography (i.e., N=0) and these for the bars with N=6, D/h_0=0.3 and $2S/L_i$=1.0 under the conditions of the lowest four resonant modes of the harbor. It is noted that in this figure, the time series of the free-surface elevation, η, at gauge G_{01} are normalized by η^*_{max} that denotes the maximum free-surface elevation during the whole simulation for the no-bar topography. The water surface inside the harbor is calm at the initial period, and the incident regular waves reach gauge G_1 after about 8~10 wave periods depending on the resonant modes. Then, the energy of the incident regular wave increases from zero to their maximum levels within approximately fifteen wave periods, regardless of the resonant mode and the number of bars. That is to say, the steady state of the harbor oscillations excited by regular long waves has already been reached at around t/T_i=25 for all the eight cases shown in this figure. In this article, only the free-surface elevations during the steady-state process (t/T_i>25) are studied and analyzed for all the cases with the incident regular long waves.

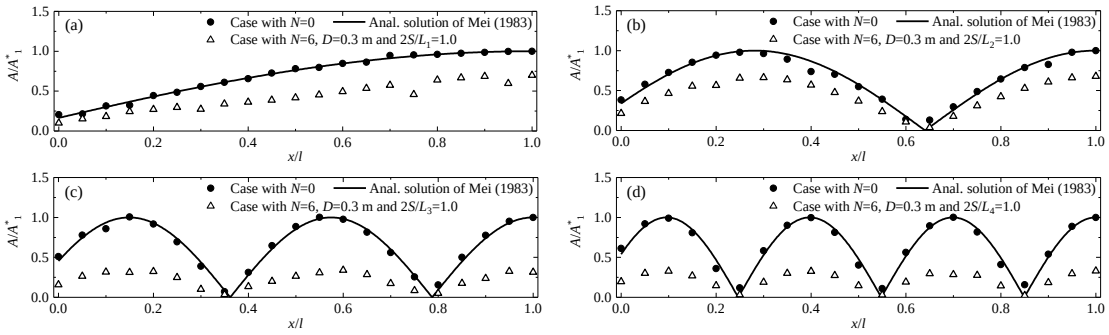

Fig. 10. The predicted amplitude distribution by the numerical model (dots) for the eight cases shown in Fig. 9 and the analytical ones by Mei (1983)'s solution (lines). (a)–(d) correspond to Modes 1–4, respectively. A denotes the response amplitudes of the regular long waves at various positions inside the harbor. A^*_1 denotes the response amplitude at gauge G_1 for the no-bar topography.

Based on the time series of the free-surface elevations during the steady-state process, the mean zero-up-crossing wave amplitudes at all gauges are calculated, and their spatial distributions inside the harbor for the eight cases in Fig. 9 are further illustrated in Fig. 10. It is noted that the spatial distributions of the wave amplitude are normalized by A^*_1 that denotes the response amplitude at gauge G_1 for the no-bar topography. For comparison, the analytical amplitude distribution based on Mei (1983)'s solution for each resonant mode is also plotted here. Three phenomena can be easily observed. Firstly, for all the four cases with N=0, because there is no bar outside the harbor, the amplitude distributions simulated by the numerical model coincides well with the analytical ones of Mei (1983), which indicates again the accuracy of the present numerical model in simulating the harbor resonance phenomenon.

Secondly, because of the total reflection at the backwall of the harbor, there always exist a maximum value of the response amplitudes there, no matter whether the patch of bars exists or not. Hence, considering the significance of the response amplitude at gauge G_1, the ratio of the response amplitude at gauge G_1 for N>0 (denoted by A_1) to that for N=0 (denoted by A^*_1) will be used as a measure to quantitatively assess the effect of sinusoidal bars on the harbor resonance.

Thirdly, for the four resonant modes, the response amplitudes inside the harbor for the cases with N=6 are shown to be always lower than the corresponding ones for the cases with N=0 to different degrees. To illustrate this point quantitatively, the amplitude ratios, A_1/A^*_1, for all the four

resonant modes are listed in Table 4. It is seen that for Modes 1 and 2, the amplitude ratios are 69.99% and 67.77%, which indicates that the intensity of the harbor resonance are reduced by about 30% due to the external sinusoidal bars. For Modes 3 and 4, the amplitude ratios decrease to 31.54% and 32.94%, respectively. This illustrates that more than 70% of the resonant amplitude inside the harbor is suppressed for these two resonant modes.

Table 4. The ratios of the response amplitudes at gauge G_1 for the cases with N=6, D=0.3 m and $2S/L_i$=1.0 to those for the cases with N=0 for Modes 1–4. A_1 in this table denotes the response amplitudes of the regular long waves at gauge G_1 for the cases with N>0.

Ratio	Mode 1	Mode 2	Mode 3	Mode 4
A_1/A^*_1 (%)	69.99	67.77	31.54	32.94

Based on the limited information presented in Fig. 10 and Table 4, it seems that Bragg resonant reflection can effectively alleviate the harbor resonance for various modes induced by the regular long waves. More comprehensive results and discussions on the effects of Bragg reflection on the harbor oscillations excited by the regular long waves will be presented in subsection 4.2.

4.1.2. Incident bichromatic short wave groups

The technique of Morlet wavelet transform is adopted here to reveal both time- and frequency-domain information from the time series of the free-surface elevation. Fig. 11 presents the time series of the free-surface elevations at gauge G_1 and the corresponding wavelet spectra for three cases in which the harbor oscillations are triggered by bichromatic short wave groups. The three cases include the no-bar topography, the long-bar type topography with N=8, D/h_0=0.3 and $2S/L_1$=1.0, and the short-bar type topography with N=8, D/h_0=0.3 and $2S/\zeta$=1.0. It is seen that both the short wave components (F_1 and F_2) and the sub-harmonic components (Δf) for all the three cases have basically approached the steady state at about t/T_1=20. Identical to the cases with the incident regular long waves, only the free-surface elevations during the steady-state process (t/T_i>25) are used for data analysis below.

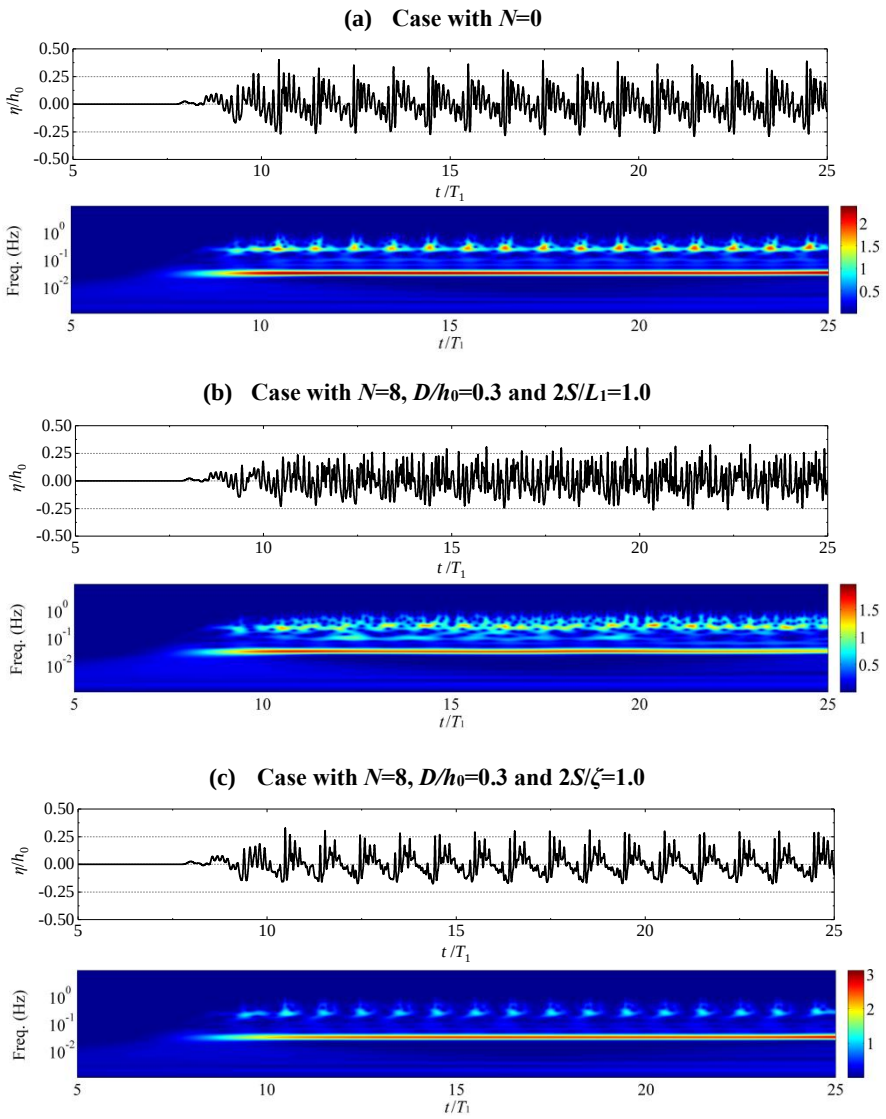

Fig. 11. Time series of the free-surface elevations at gauge G_1 and the corresponding wavelet spectra for three cases in which the harbor oscillations are triggered by incident bichromatic short wave groups.

Based on the technique of the discrete Fourier transform, the response amplitudes of the sub-harmonic component at all gauges are extracted from the steady-state time series of the free-surface elevations. Fig. 12 demonstrates the spatial distributions of the amplitude of the sub-harmonic component inside the harbor for the three cases in Fig. 11. A_L in this figure denotes the amplitude of the sub-harmonic component at various positions inside the harbor, and A^*_{L1} denotes its amplitude at gauge G_1 for the no-bar topography. Similar to Fig. 10, due to the total reflection at the backwall of the harbor, the maximum response amplitude always occurs there; hence, the ratio of the sub-harmonic amplitude at gauge G_1 for $N>0$ (denoted by A_{L1}) to that for $N=0$ (i.e., A^*_{L1}) will be used as an indicator to estimate the effect of sinusoidal bars on the harbor oscillations excited by bichromatic

short wave groups.

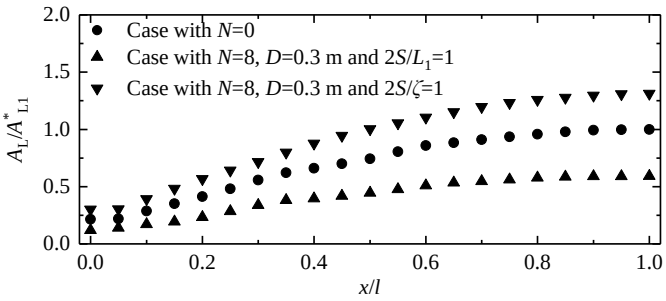

Fig. 12. Spatial distributions of the amplitude of the sub-harmonic component inside the harbor for the three cases shown in Fig. 11. A_L denotes the amplitude of the sub-harmonic component at various positions inside the harbor. A^*_{L1} denotes its response amplitude at gauge G_1 for no sinusoidal-bar topography.

It can also be observed from Fig. 12 that the long-bar type topography with N=8, D/h_0=0.3 and $2S/L_1$=1.0 can significantly decrease the amplitude of the sub-harmonic component inside the whole harbor, and the amplitude ratio A_{L1}/A^*_{L1} is 59.14%. However， for the short-bar type topography with N=8, D/h_0=0.3 and $2S/\zeta$=1.0, the amplitude of the sub-harmonic component inside the harbor is enhanced to a certain degree, and the value of A_{L1}/A^*_{L1} is 131.25%. These indicate that the long-bar type topography seems to be able to relieve the nonlinear harbor oscillations triggered by the bichromatic wave groups, while it does not seem to work for the short-bar type topography. More results and discussion on the influences of Bragg reflection on the harbor oscillations excited by the bichromatic wave groups will be demonstrated in subsection 4.3.

4.2. Effects on the harbor oscillations excited by the incident regular long waves

The overall results on the harbor oscillations excited by the regular long waves are first presented in subsection 4.2.1, and the capacity of Bragg reflection to mitigate the strength of harbor resonance is first revealed there. Then, the effects of the number and the amplitude of the sinusoidal bars are investigated in subsections 4.2.2 and 4.2.3, respectively. Finally, the sensitivity of the research findings to the resonant mode of the harbor is discussed in subsection 4.2.4.

4.2.1. Overall results for the effects of Bragg reflection

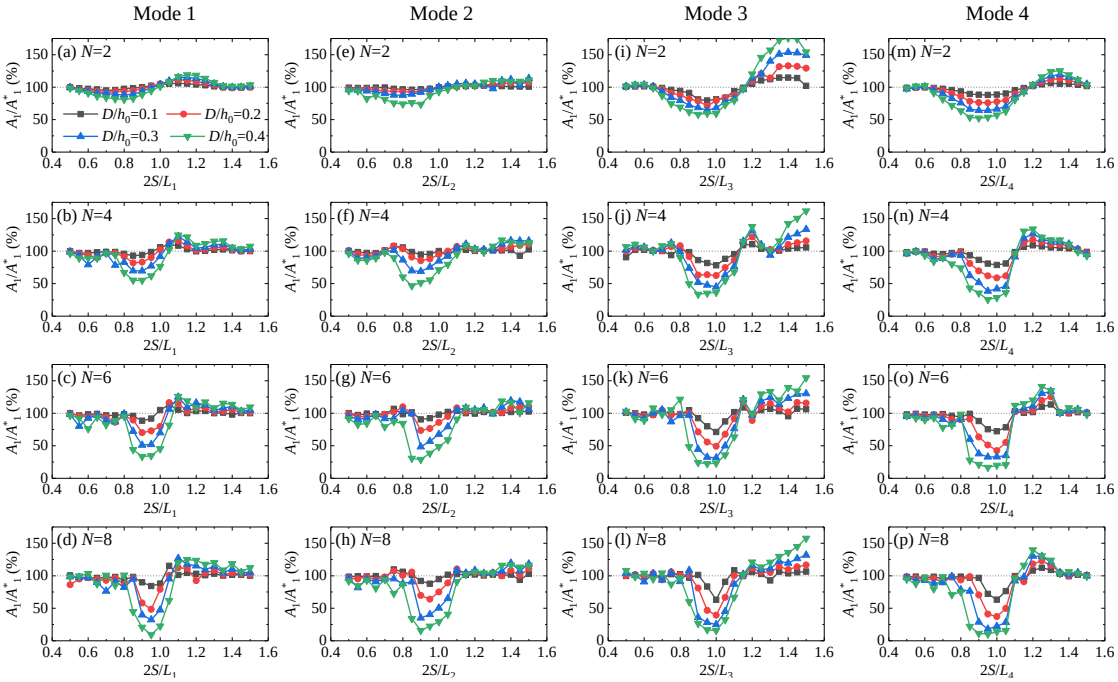

Fig. 13. Variations of A_1/A^*_1 with respect to $2S/L_i$ under conditions of different numbers of bars for Mode 1 (a–d), Mode 2 (e–h), Mode 3 (i–l), and Mode 4 (m–p).

Fig. 13 presents the variations of A_1/A^*_1 with respect to $2S/L_i$ (i=1, 2, 3, and 4) under conditions of different numbers of bars for the lowest four resonant modes. Three obvious phenomena can be observed. Firstly, at the vicinity of $2S/L_i$=1, the values of A_1/A^*_1 are always significantly less than 100%. It indicates that the patch of periodic bar topographies can remarkably mitigate the harbor resonance induced directly by the regular long waves when Bragg resonant reflection occurs. It has been pointed out in the Introduction that, on the one hand, Bragg reflection can significantly decrease the wave energy propagating into the harbor and is beneficial to alleviate harbor oscillations; on the other hand, the periodic undulation could also significantly reflect the radiated waves back into the harbor and aggravate harbor resonance. It is obvious that the alleviating effect of the periodic bars are always stronger than its aggravating effect when Bragg resonant reflection occurs.

The probable reason for this phenomenon is as follows. The incident waves from the open sea propagate orthogonally to the bars. This is the perfect condition for the incident waves to undergo Bragg resonant reflection, which causes that only a very small proportion of the incident wave

energy enters the harbour. However, the radiated waves are mostly cylindrical with respect to the origin at the harbor entrance. They propagate with a variable direction with the bars and are not in the optimal condition for Bragg reflection. Furthermore, the radiated waves reflected by the bars do not go back directly into the harbor, but more likely attack the surrounding coastline.

Secondly, the sinusoidal bars tend to intensify harbor oscillations when $2S/L_i$ is approximately larger than 1.15. Under this condition, the alleviating effect of the periodic bars becomes weaker than its aggravating effect. Thirdly, both the minimum value of A_1/A^*_1 (denoted by the symbol "$(A_1/A^*_1)_m$" hereinafter) and its corresponding value of $2S/L_i$ (called as the optimal normalized wavelength of the undulating topography and denoted by the symbol "$(2S/L_i)_m$") for each set of N, D and the resonant mode are closely related to the geometrical parameters of the bars and to the resonant mode. More detailed discussions on how the geometrical parameters of the bars and the resonant mode affect them will be shown in subsections 4.2.2-4.2.4.

4.2.2. The effects of the number of bars

It is obvious that the value of $(A_1/A^*_1)_m$ can quantitatively embody the mitigation effect of Bragg reflection on the harbor resonance induced directly by regular long waves, and that a lower $(A_1/A^*_1)_m$ indicates the better mitigation effect. The variations of $(A_1/A^*_1)_m$ with respect to the number of bars, N, for various resonant modes are demonstrated in Fig. 14. It is seen that for all the lowest four resonant modes, $(A_1/A^*_1)_m$ decreases with the increase of the bar number, regardless of the bar amplitude. Moreover, in general, this downward trend seems to be linear in the variation range of the parameters considered in this article. This indicates that when Bragg resonant reflection occurs, the alleviating effect of the periodic bars on various resonant modes of the harbor triggered by regular long waves is linearly enhanced as the bar number increases.

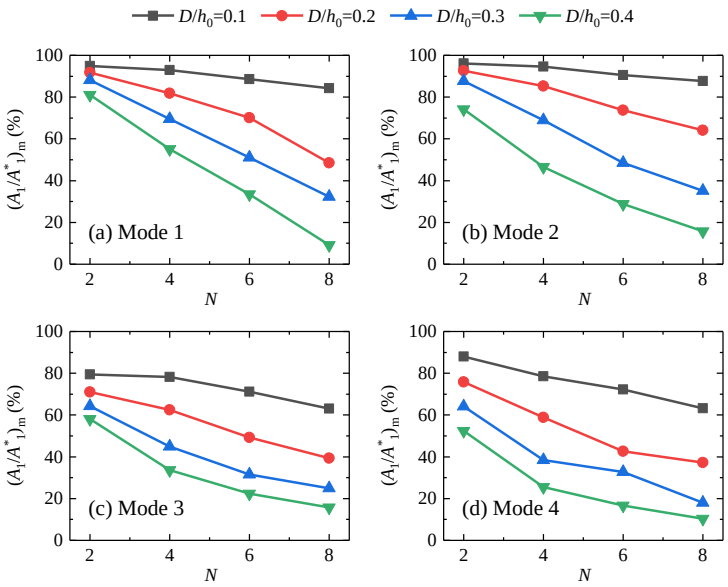

Fig. 14. Variations of $(A_1/A^*_1)_m$ with respect to the number of bars, N, for various resonant modes.

The recognition on the optimal normalized wavelength of the undulating topography, $(2S/L_i)_m$, is also vitally important because it can accurately tell coastal engineers what kind of geometric conditions can achieve the best mitigation effect on harbor oscillations. Fig. 15 presents the variations of $(2S/L_i)_m$ with respect to the number of bars, N, for various resonant modes. Three phenomena can be easily seen from this figure. Firstly, the value of $(2S/L_i)_m$ is not always exactly equal to 1.0. For most cases, its value is less than 1.0. This downward shift of $(2S/L_i)_m$ from 1.0 was also frequently found in the investigations for the pure Bragg reflection phenomenon (e.g. Guazzelli et al. (1992); Liu et al. (2019a); Liu et al. (2020); Peng et al. (2019)). Secondly, the value of $(2S/L_i)_m$ is shown to gradually increase with the increase of N, which is also consistent with the theoretical finding of Liu et al. (2019a) for pure Bragg reflection (see Table 2 in Liu et al. (2019a)). These two phenomena indicate that Bragg resonant reflection plays a dominant role in the coupling interactions between the patch of sinusoidal bars and the harbor.

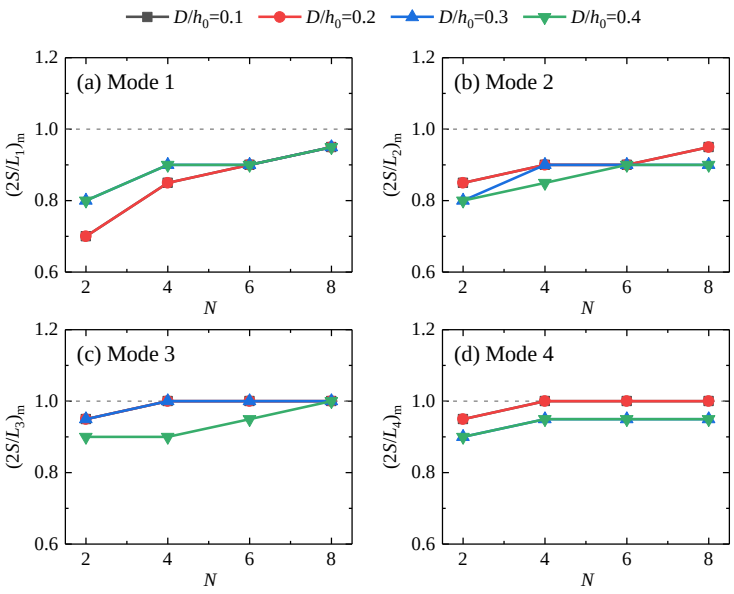

Fig. 15. Variations of $(2S/L_i)_m$ with respect to the number of bars, N, for various resonant modes.

Thirdly, compared to Modes 3 and 4, the values of $(2S/L_i)_m$ for Modes 1 and 2 deviate from 1.0 more remarkably. Moreover, the values of $(2S/L_i)_m$ for Modes 1 and 2 are shown to be more sensitive to the number of bars. For better illustration, Modes 1 and 4 are taken for examples here. For Mode 1, the variation range of $(2S/L_i)_m$ is from 0.70 to 0.95, and the difference between the upper and the lower limits is 0.25; while for Mode 4, its variation range is from 0.90 to 1.0, and the difference between the upper and the lower limits is only 0.10. It can be qualitatively explained as follows. For both Modes 1 and 2, their intensities of harbor oscillations are significantly stronger than those of Modes 3 and 4 (see Fig. 7). Therefore, the energy of the radiated waves for the former two modes are much higher than that for the latter two modes; the modulatory effects of the radiated waves on Bragg reflection for the former two modes are significantly stronger those for the latter two modes. Hence, it well explains why $(2S/L_i)_m$ deviates from 1.0 more notably and is more sensitive to N for Modes 1 and 2.

4.2.3. The effects of the amplitudes of bars

The variations of $(A_1/A^*_1)_m$ with respect to the normalized amplitude of bars, D/h_0, for the lowest four resonant modes are presented in Fig. 16. Similar to the phenomena in Fig. 14, $(A_1/A^*_1)_m$ is shown to decrease linearly with the bar amplitude overall, regardless of the resonant mode and the bar number, which shows that the alleviating effect of Bragg reflection on the harbor resonance

excited directly by regular long waves is also linearly improved as the bar amplitude increases.

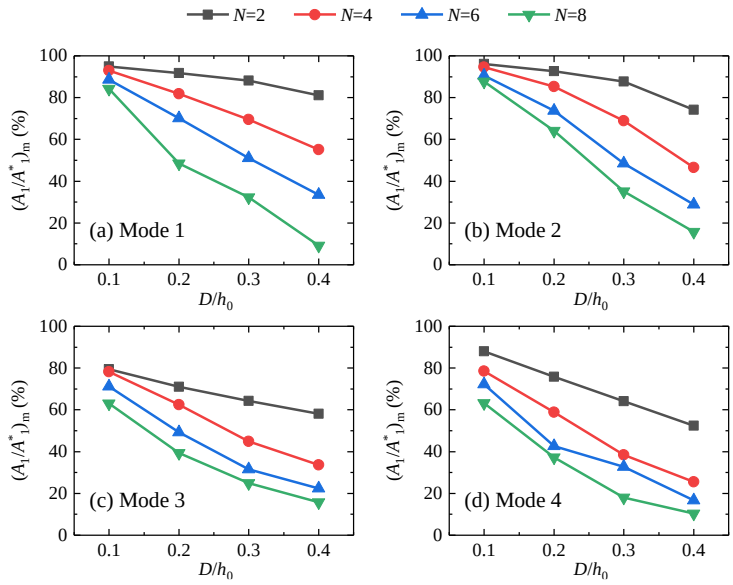

Fig. 16. Variation of $(A_1/A^*_1)_m$ with respect to the normalized amplitude of bars, D/h_0, for various resonant modes.

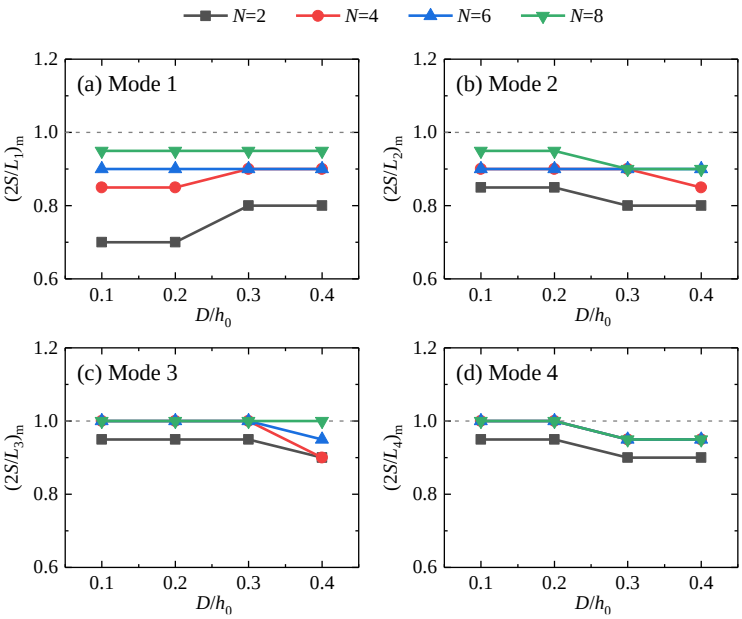

Fig. 17. Variation of $(2S/L_i)_m$ with respect to the normalized amplitude of bars, D/h_0, for various resonant modes.

Fig. 17 further presents the variation of $(2S/L_i)_m$ with respect to the normalized amplitude of bars, D/h_0, for various resonant modes. Different from the consistent changing trends of $(2S/L_i)_m$

with N for all the four modes shown in Fig. 15, the effect of the amplitude of bars on $(2S/L_i)_m$ depends closely on the resonant mode. Specifically speaking, for Mode 1, the increase of D/h_0 tends to cause the increase of $(2S/L_i)_m$; while for Modes 2-4, the rise of D/h_0 is inclined to decrease the value of $(2S/L_i)_m$.

4.2.4. The effects of the resonant mode

The sensitivities of both $(A_1/A^*_1)_m$ and $(2S/L_i)_m$ to different resonant modes of the harbor are presented in Figs. 18 and 19, respectively. In general, $(A_1/A^*_1)_m$ is shown to decrease with the increase of the resonant mode although there exist some fluctuations under the conditions of D/h_0=0.1 and 0.2 (see Fig. 18). On the contrary, $(2S/L_i)_m$ is shown to increase with the resonant mode overall, although there also are some fluctuations for D/h_0=0.3 and 0.4 (see Fig. 19). It means that the value of $(2S/L_i)_m$ becomes closer to 1.0 as the resonant mode rises, which is consistent with the related finding in Fig. 15.

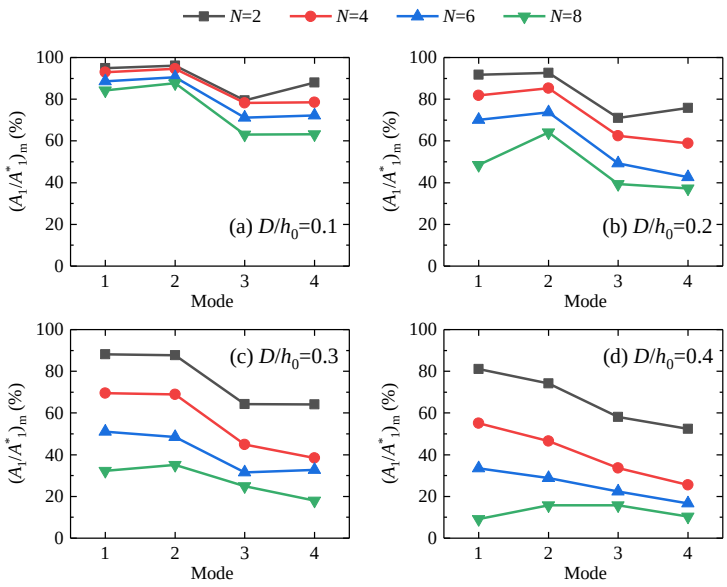

Fig. 18. Variations of $(A_1/A^*_1)_m$ with respect to the resonant mode for various amplitudes of bars

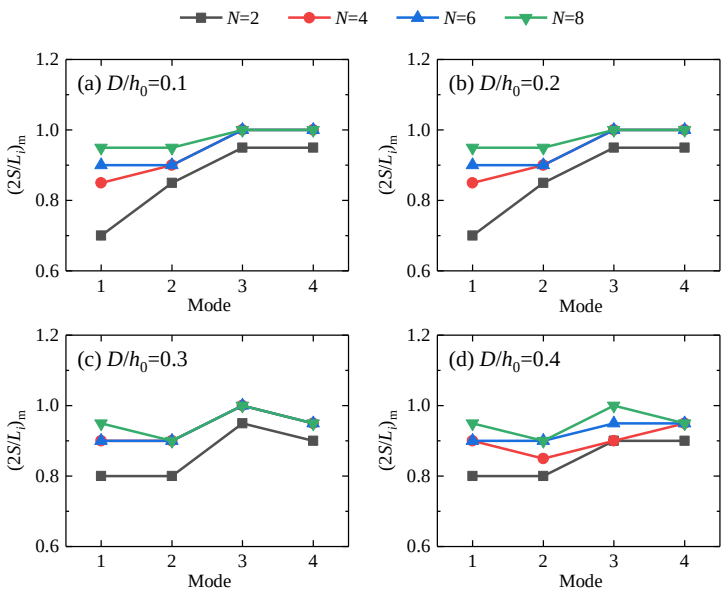

Fig. 19. Variations of $(2S/L_i)_m$ with respect to the resonant mode for various amplitudes of bars

4.3. Effects on the harbor oscillations induced by the incident bichromatic short wave groups

The overall results on the harbor resonance induced by incident bichromatic short wave groups over both types of topographies (i.e., the long-bar and the short-bar type) are first presented in subsection 4.3.1. Then, aiming at the long-bar type topography, the effects of the number and the amplitude of the bars are revealed in subsections 4.3.2 and 4.3.3, respectively.

4.3.1. Overall results for the effects of Bragg reflection

Fig. 20 demonstrates the variations of A_{L1}/A^*_{L1} with respect to $2S/L_1$ (for the long-bar type topography) and to $2S/\zeta$ (for the short-bar type topography) under conditions of various numbers and amplitudes of bars. It is seen that the long-bar type topography has the capacity of alleviating the nonlinear harbor oscillations induced by the bichromatic short wave groups when the value of $2S/L_1$ is in the vicinity of 1.0. In the ranges of the parameters of the long-bar type topography considered, the strength of the nonlinear harbor oscillations can be weakened by up to 76.4% for the case with N=8, D/h_0=0.4 and $2S/L_1$=0.95 where A_{L1}/A^*_{L1} is only 23.6% (see Fig. 20d). For the short-bar type topography, it seems that it can also play a certain role in alleviating the nonlinear harbor resonance when the value of $2S/\zeta$ is around 1.0. However, compared to the long-bar type topography, the mitigation effect of the short-bar type topography is much weaker. At the ranges of the parameters of the short-bar type topography considered, the strength of the nonlinear harbor oscillations can be weakened only by 23.0% for the case with N=8, D/h_0=0.2 and $2S/L_1$=0.95 where

A_{L1}/A^*_{L1} is 77.0% (see Fig. 20h).

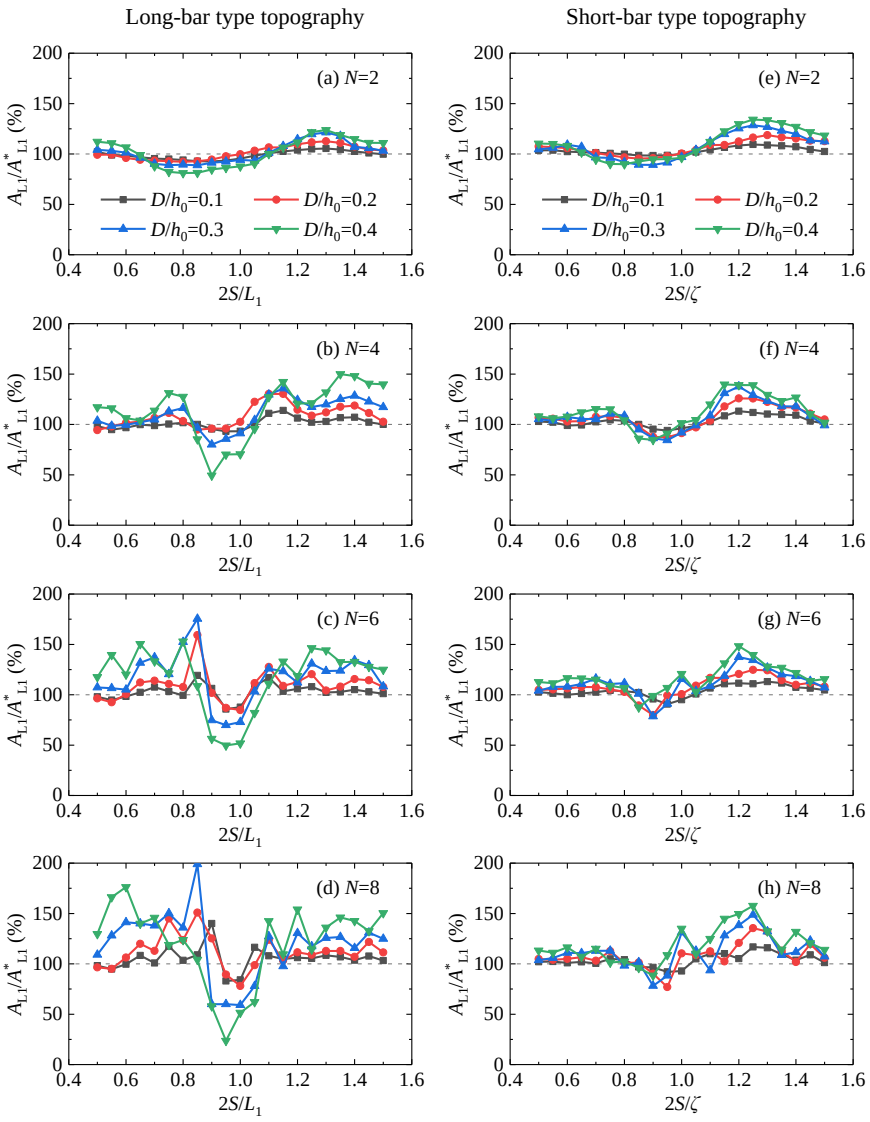

Fig. 20. Variations of A_{L1}/A^*_{L1} with respect to the wavelength of sinusoidal bars: (a-d) correspond to long-bar type topographies with various bar numbers; (e-h) correspond to short-bar type topographies with various bar numbers.

More discussions on how the geometrical parameters of the bars influence the minimum value of A_{L1}/A^*_{L1} (denoted by the symbol "$(A_{L1}/A^*_{L1})_m$" hereinafter) and the optimal normalized wavelength of the bars for each set of N and D will be demonstrated in subsections 4.3.2 and 4.3.3. In view of the effectiveness of the long-bar type topography on mitigating nonlinear harbor oscillations, the discussions will focus only on this type of topography.

4.3.2. The effects of the number of bars

Fig. 21 presents the variations of $(A_{L1}/A^*_{L1})_m$ and $(2S/L_1)_m$ with respect to the number of bars, N, for the long-bar type topography. It is seen that for $(A_{L1}/A^*_{L1})_m$ (Fig. 21a), its value declines with the increase of the bar number overall, which indicates that the mitigation effect of Bragg reflection on the nonlinear harbor oscillations becomes better and better as N rises. This phenomenon is similar to that shown in Fig. 14 where the harbor resonance triggered by regular long waves is concerned. For $(2S/L_1)_m$ (Fig. 21b), its value is shown to increase gradually with the increase of N and its variation range is from 0.80 to 1.0, which is like the phenomenon illustrated in Fig. 15.

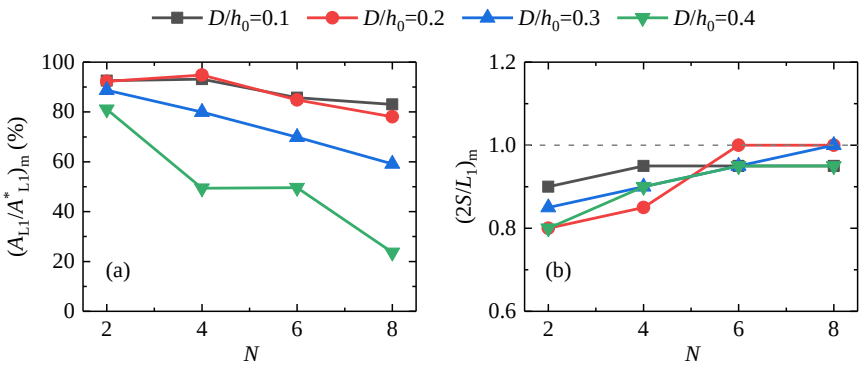

Fig. 21. Variations of $(A_{L1}/A^*_{L1})_m$ and $(2S/L_1)_m$ with respect to the number of bars, N, for the long-bar type topography. (a) and (b) correspond to $(A_{L1}/A^*_{L1})_m$ and $(2S/L_1)_m$, respectively.

4.3.3. The effects of the amplitudes of bars

Fig. 22 demonstrates the variations of $(A_{L1}/A^*_{L1})_m$ and $(2S/L_1)_m$ with respect to the normalized amplitudes of bars, D/h_0, for the long-bar type topography. In general, the value of $(A_{L1}/A^*_{L1})_m$ decreases with the increase of the bar amplitudes (Fig. 22a), which shows that the mitigation effect on the nonlinear harbor oscillations becomes better as the bar amplitude increases. The phenomenon is similar to that shown in Fig. 16. While for $(2S/L_1)_m$ (Fig. 22b), as the bar amplitude increases, it always fluctuates around certain values that depend on the bar number.

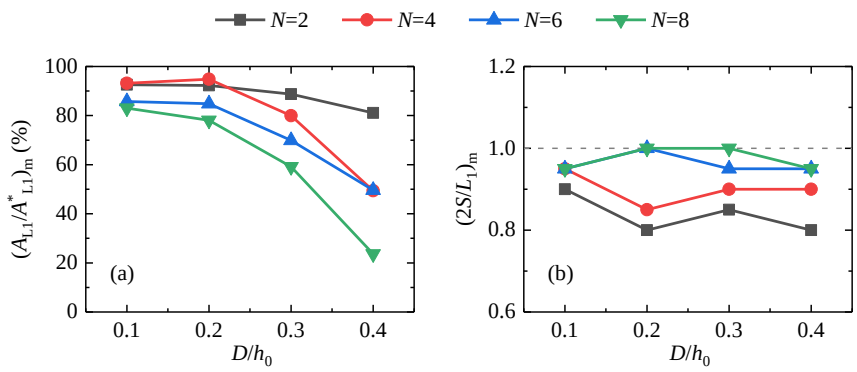

Fig. 22. Variations of $(A_{L1}/A^*_{L1})_m$ and $(2S/L_1)_m$ with respect to the amplitude of bars for the long-bar type topography. (a) and (b) correspond to $(A_{L1}/A^*_{L1})_m$ and $(2S/L_1)_m$, respectively.

5. Conclusions and implications

5.1. Conclusions

In this article, the coupling interactions between the incident steady-state waves, the harbor, and the patch of sinusoidal bars outside the harbor are studied for the first time by utilizing the fully nonlinear Boussinesq model, FUNWAVE 2.0. The incident steady-state waves considered include regular long waves and bichromatic short wave groups. Correspondingly, two kinds of harbor oscillations, that is, the harbor resonance triggered directly by the regular long waves and the nonlinear harbor resonance induced by the bichromatic short wave groups, are studied in the present study. For the first kind of harbor oscillations, the effects of the sinusoidal bars on the lowest four resonant modes are systematically investigated. For the second kind, two types of bar topographies (i.e., the long-bar and the short-bar types) are studied, and only the lowest resonant mode of the harbor is studied. The capability of Bragg reflection to alleviate both kinds of harbor oscillations is revealed first. Subsequently, the effects of the geometrical parameters (including the number and the amplitude of bars) on the best mitigation effect for harbor resonance and on the optimal wavelength of bars that can achieve the best mitigation effect are comprehensively investigated. The results of the current research have broadened the knowledge on the harbor oscillations excited by the steady-state wave conditions.

The following main conclusions can be drawn from the results of this study:

(1) The patch of periodic bar topographies can remarkably mitigate the harbor oscillations induced directly by the regular long waves when Bragg resonant reflection occurs. Under this condition, the alleviating effect of the periodic bars resulting from the remarkable reflection of the incident

waves are always stronger than its aggravating effect caused by the reflection of the radiated waves back into the harbor, which indicates that Bragg resonant reflection always dominates the coupling process. On the other hand, the radiated waves from the harbor entrance also play a modulation role to a certain extent, especially for the lowest two resonant modes of the harbor.

(2) When Bragg resonant reflection occurs, the alleviating effect of the sinusoidal bars on the harbor resonance excited by regular long waves is linearly enhanced as the number or the amplitude of bars increases. The optimal normalized wavelength of bars denoted by $(2S/L_i)_m$ (i=1, 2, 3, and 4) is not always exactly equal to 1.0. For most cases, its value is less than 1.0. Moreover, the value of $(2S/L_i)_m$ is shown to gradually increase with the bar number, regardless of the resonant mode of the harbor. However, the effect of the bar amplitude on $(2S/L_i)_m$ depends closely on the resonant mode. For Mode 1, the increase of the amplitude tends to cause the increase of $(2S/L_i)_m$; while for Modes 2-4, the rise of the amplitude is inclined to decrease the value of $(2S/L_i)_m$.

(3) The long-bar type topography has the capacity of alleviating the nonlinear harbor oscillations induced by the bichromatic short wave groups effectively when Bragg resonant reflection occurs. In the variation ranges of the parameters of the long-bar type topography considered, the strength of the nonlinear harbor oscillations can be weakened by up to 76.4%. However, for the short-bar type topography, its capability of mitigating the nonlinear harbor resonance is limited. In the ranges of the parameters of the short-bar type topography, the strength of the nonlinear harbor oscillations can be weakened only by 23.0%.

(4) Like the harbor resonance triggered directly by the regular long waves, the alleviating effect of the long-bar type topography on the nonlinear harbor resonance induced by the bichromatic wave groups becomes better and better as the number or the amplitude of bars increases, and the optimal normalized wavelength of the long-bar type topography denoted by $(2S/L_1)_m$ also increases gradually with the number of bars. However, $(2S/L_1)_m$ is always shown to fluctuate with the amplitude of bars around certain values that depend on the number of bars.

(5) For most cases, the optimal normalized wavelength of bars is less than 1.0, rather than exactly equal to 1.0, no matter for the harbor resonance triggered directly by the regular long waves or the nonlinear harbor resonance induced by the bichromatic wave groups. This downward shift of the optimal normalized wavelength of bars is consistent with the related finding in the investigations of the pure Bragg reflection phenomenon.

We reaffirm here that the above-mentioned conclusions are only valid for the given harbor, incident wave parameters and resonant modes, and the variation ranges of the geometrical parameters of the sinusoidal bars considered in this article.

5.2. Implications

Based on the above conclusions, the following implications can be obtained in the practice:

(1) To mitigate the long-period resonance in a built harbor is very tough and expensive (Lee and Xing, 2009). Alteration of the general layout is one option, but sometimes it seems impossible, especially for a built harbor. The present research proposes a new option: to change the bottom profile to use the Bragg reflection to mitigate the harbor resonance, which is much more feasible as long as the navigating depth is guaranteed.

(2) If there are natural bars at the location of a harbor to be built, the possible countermeasure and its mitigation effect on harbor resonance depend on the wavelength of the natural bars. For the bar wavelength, S, with the order of tens of meters to hundreds of meters, the general layout of the harbor needs to be carefully designed based on the following principle. That is, the wavelength of the incident long waves that correspond to the most destructive resonant mode, L_i, should approach the value of $(2S/L_i)_m$ as closely as possible. In general, to meet the above principle, a trial-and-error designing process is inevitable.

(3) For the natural bars with the wavelength ranging only from meters to more than ten meters, the natural bars should be artificially modified (if needed) so that their wavelength approaches the value of $(2S/\zeta)_m$ as closely as possible. $(2S/\zeta)_m$ denotes the optimal normalized wavelength of the short-type bars that can achieve $(A_{L1}/A^*_{L1})_m$ (refer to Fig. 20e-h). ζ here corresponds to the short wavelength of the spectral peak period. This countermeasure could also alleviate the harbor resonance to a certain extent, although its mitigation effect is not as good as that of the above-mentioned long-type bars with much longer wavelengths.

(4) For built harbors without natural bars, the artificial bars could be arranged outside the harbor entrance. The designing principles of the artificial bars are similar to those presented in the implications (1) and (2) and are not repeated here. Compared to the natural bars, the artificial bars are more suitable for small-scale harbors (e.g., the marina). This is because, for large-scale harbors, if the relationship of $(2S/L_i)_m$ was satisfied, the value of S might be too large to make

such artificial bars in the practical engineering.

(5) Based on the investigations for the pure Bragg reflection, it has been found that not only the sinusoidal bars but also the artificial bars with other section forms (e.g., rectangle, trapezoid, and triangle) can result in the Bragg resonant reflection. Hence, it can be reasonably inferred that, like the sinusoidal bars, these artificial bars are probably capable of alleviating harbor oscillations. Compared to the sinusoidal bars, these artificial bars are more suitable for the actual engineering because they are easier to be manufactured. However, the mitigation effect of these artificial bars needs to be further investigated in the future.

Acknowledgments

This research is financially supported by the National Natural Science Foundation of China (Grant Nos. 52071060 and 51809039), the Natural Science Foundation of Jiangsu Province (Grant No. BK20201455), the Natural Science Foundation of the Jiangsu Higher Education Institutions (Grant No. 20KJD170005) and the Qing Lan Project of Jiangsu Universities. The work is also partially supported by UK EPSRC (Grant No. EP/T026782/1), the Royal Academy of Engineering (Grant No. UK-CIAPP/73) and the Royal Society (Grant No. IEC\NSFC\181321).

References

Araújo, R., Alfredini, P., Amaral, R.F.D., 2004. Sand Waves of the Navigation Channel of the Ponta da Madeira Harbour (Brazil) Proceedings of the 29th Conference on Coastal Engineering, Lisbon, Portugal, pp. 2558-2567.

Bellotti, G., 2007. Transient response of harbours to long waves under resonance conditions. Coastal Engineering 54 (9), 680-693.

Boczar-Karakiewicz, B., Davidson-Arnott, R.G.D., 1987. Nearshore bar formation by non-linear wave processes - A comparison of model results and field data. Marine Geology 77, 287–304.

Bruno, D., Serio, F.D., Mossa, M., 2009. The FUNWAVE model application and its validation using laboratory data. Coastal Engineering 56 (7), 773-787.

Chawla, A., Kirby, J.T., 2000. A source function method for generation of waves on currents in Boussinesq models Applied Ocean Research 22 (2), 75-83.

Davies, A.G., Heathershaw, A.D., 1984. Surface-wave propagation over sinusoidally varying topography. Journal of Fluid Mechanics 144, 419-443.

De Jong, M.P.C., Battjes, J.A., 2004. Seiche characteristics of Rotterdam Harbour. Coastal Engineering 51 (5-6), 373-386.

Dolan, T.J., Dean, R.G., 1985. Multiple longshore sand bars in the upper Chesapeake Bay. Estuarine, Coastal and Shelf Science 21 (5), 727-743.

Elgar, S., 2003. Bragg reflection of ocean waves from sandbars. Geophysical Research Letters 30 (1), 1016.

Endoh, T., Inazu, D., Waseda, T., Hibiya, T., 2018. A parameter quantifying radiation damping of bay oscillations excited by incident tsunamis. Continental Shelf Research 157, 10-19.

Fabrikant, A.L., 1995. Harbor oscillations generated by shear flow. Journal of Fluid Mechanics 282, 203-217.

Gao, J., Ji, C., Gaidai, O., Liu, Y., Ma, X., 2017a. Numerical investigation of transient harbor oscillations induced by N-waves. Coastal Engineering 125, 119-131.

Gao, J., Ji, C., Liu, Y., Ma, X., Gaidai, O., 2017b. Influence of offshore topography on the amplification of infragravity oscillations within a harbor. Applied Ocean Research 65, 129-141.

Gao, J., Ma, X., Chen, H., Zang, J., Dong, G., 2021. On hydrodynamic characteristics of transient harbor resonance excited by double solitary waves. Ocean Engineering 219, 108345.

Gao, J., Ma, X., Dong, G., Zang, J., Zhou, X., Zhou, L., 2019a. Topographic influences on transient harbor oscillations excited by N-waves. Ocean Engineering 192, 106548.

Gao, J., Ma, X., Zang, J., Dong, G., Ma, X., Zhu, Y., Zhou, L., 2020. Numerical investigation of harbor oscillations induced by focused transient wave groups. Coastal Engineering 158, 103670.

Gao, J., Zhou, X., Zang, J., Chen, Q., Zhou, L., 2018. Influence of offshore fringing reefs on infragravity period oscillations within a harbor. Ocean Engineering 158, 286-298.

Gao, J., Zhou, X., Zhou, L., Zang, J., Chen, H., 2019b. Numerical investigation on effects of fringing reefs on low-frequency oscillations within a harbor. Ocean Engineering 172, 86-95.

Goda, Y., Suzuki, T., 1976. Estimation of incident and reflected waves in random wave experiments, Proceedings of the 15th Coastal Engineering Conference, Honolulu, Hawaii, pp. 828-845.

Guazzelli, E., Rey, V., Belzons, M., 1992. Higher-order Bragg reflection of gravity surface waves

by periodic beds. Journal of Fluid Mechanics, 245, 301-317.

Gulshan, Kumar, P., Rajni, 2020. Moored ship motion analysis in Paradip port under the resonance conditions using 3-D boundary element method. Journal of Marine Science and Technology 25, 1075-1092.

Guo, F.-C., Liu, H.-W., Pan, J.-j., 2021. Phase downshift or upshift of Bragg resonance for water wave reflection by an array of cycloidal bars or trenches. Wave Motion 106, 102794.

Hsu, T.-W., Hsiao, S.-C., Ou, S.-H., Wang, S.-K., Yang, B.-D., Chou, S.-E., 2007. An application of Boussinesq equations to Bragg reflection of irregular waves. Ocean Engineering 34 (5-6), 870-883.

Ippen, A.T., Goda, Y., 1963. Wave Induced Oscillations in Harbors: The Solution for a Rectangular Harbor Connected to The Open Sea. Hydrodynamics Laboratory, Massachusettes Institute of Technology, Washington, D. C.

Kar, P., Koley, S., Sahoo, T., 2020. Bragg scattering of long waves by an array of trenches. Ocean Engineering 198, 107004.

Kennedy, A.B., Kirby, J.T., Chen, Q., Dalrymple, R.A., 2001. Boussinesq-type equations with improved nonlinear performance. Wave Motion 33, 225-243.

Kirby, J.T., Anton, J.P., 1990. Bragg reflection of waves by artificial bars, Proceedings of the 22nd International Conference on Coastal Engineering, New York, pp. 757–768.

Kirby, J.T., Long, W., Shi, F., 2003. Funwave 2.0 Fully Nonlinear Boussinesq Wave Model On Curvilinear Coordinates. Report No. CACR-02-xx. Center for Applied Coastal Research, Dept. of Civil & Environmental Engineering, University of Delaware, Newark, Delaware.

Knapp, R.T., Vanoni, V.A., 1945. Wave and surge study for the Naval Operating Base, Terminal Island, Callfornia. California Institute of Technology, Pasadena, CA.

Kumar, P., Gulshan, 2017. Extreme wave-induced oscillation in Paradip Port under the resonance conditions. Pure and Applied Geophysics 174 (2), 4501-4516.

Kumar, P., Gulshan, 2018. Theoretical analysis of extreme wave oscillation in Paradip Port using a 3-D boundary element method. Ocean Engineering 164, 13-22.

Kumar, P., Zhang, H., Kim, K.I., Yuen, D.A., 2016. Modeling wave and spectral characteristics of moored ship motion in Pohang New Harbor under the resonance conditions. Ocean Engineering 119, 101-113.

Lee, J.J., 1971. Wave induced oscillations in harbors of arbitrary geometry. Journal of Fluid Mechanics 45, 375-394.

Lee, J.J., Xing, X., 2009. Computer Modeling for Harbor Planning and Design, in: Kim, Y.C. (Ed.), Handbook of Coastal and Ocean Engineering. World Scientific Publishing, Singapore, pp. 695-722.

Li, A.-j., Liu, Y., Liu, X., Zhao, Y., 2020. Analytical and experimental studies on Bragg scattering of water waves by multiple submerged perforated semi-circular breakwaters. Ocean Engineering 209, 107419.

Liu, H.-W., 2017. Band gaps for Bloch waves over an infinite array of trapezoidal bars and triangular bars in shallow water. Ocean Engineering 130, 72-82.

Liu, H.-W., Li, X.-F., Lin, P., 2019a. Analytical study of Bragg resonance by singly periodic sinusoidal ripples based on the modified mild-slope equation. Coastal Engineering 150, 121–134.

Liu, H.-W., Luo, H., Zeng, H.-D., 2015. Optimal collocation of three kinds of Bragg breakwaters for Bragg resonant reflection by long waves. Journal of Waterway, Port, Coastal, and Ocean Engineering 114 (3), 04014039.

Liu, H.-W., Zeng, H.-D., Huang, H.-D., 2020. Bragg resonant reflection of surface waves from deep water to shallow water by a finite array of trapezoidal bars. Applied Ocean Research 94, 101976.

Liu, W., Liu, Y., Zhao, X., 2019b. Numerical study of Bragg reflection of regular water waves over fringing reefs based on a Boussinesq model. Ocean Engineering 190, 106415.

Losada, I.J., Gonzalez-Ondina, J.M., Diaz-Hernandez, G., Gonzalez, E.M., 2008. Numerical modeling of nonlinear resonance of semi-enclosed water bodies: Description and experimental validation. Coastal Engineering 55, 21-34.

Mei, C.C., 1983. The Applied Dynamics of Ocean Surface Waves. Wiley, New York.

Miles, J.W., Chamberlain, P.G., 1998. Topographical scattering of gravity waves. Journal of Fluid Mechanics 361, 175-188.

Mogi, A., 1965. Sand Waves in Kesennuma Harbour. Annals of The Tohoku Geographycal Asocciation 17 (4), 219.

Okihiro, M., Guza, R.T., 1996. Observations of seiche forcing and amplification in three small

harbors. Journal of Waterway, Port, Coastal and Ocean Engineering 122 (5), 232-238.

Peng, J., Tao, A., Liu, Y., Zheng, J., Zhang, J., Wang, R., 2019. A laboratory study of class III Bragg resonance of gravity surface waves by periodic beds. Physics of Fluids 31, 067110.

Rabinovich, A.B., 2009. Seiches and harbor oscillations, in: Kim, Y. (Ed.), Handbook of Coastal and Ocean Engineering. World Scientific Publishing, Singapore, pp. 193-236.

Rogers, S.R., Mei, C.C., 1978. Nonlinear resonant excitation of a long and narrow bay. Journal of Fluid Mechanics 88 (1), 161-180.

Russell, K.S., 1982. Coastal Engineering in South Africa, Proceedings of the 18th International Conference on Coastal Engineering, Cape Town, South Africa.

Vanoni, V.A., Carr, J.H., 1950. Harbor surging, Proceedings of the 1st International Conference on Coastal Engineering, Long Beach, pp. 60-68.

Wang, G., Zheng, J., Liang, Q., Zheng, Y., 2014. Analytical solutions for oscillations in a harbor with a hyperbolic-cosine squared bottom. Ocean Engineering 83, 16-23.

Wei, G., Kirby, J.T., Grilli, S.T., Subramanya, R., 1995. A fully nonlinear Boussinesq model for surface waves. Part 1. Highly nonlinear unsteady waves. Journal of Fluid Mechanics 294, 71-92.

Zeng, H., Qin, B., Zhang, J., 2017. Optimal collocation of Bragg breakwaters with rectangular bars on sloping seabed for Bragg resonant reflection by long waves. Ocean Engineering 130, 156-165

Zhang, J.-S., Jeng, D.-S., Liu, P.L.-F., Zhang, C., Zhang, Y., 2012. Response of a porous seabed to water waves over permeable submerged breakwaters with Bragg reflection. Ocean Engineering 43, 1-12.

Zheng, J., Yu, H., Tao, A., Fan, J., Wang, Y., 2016. Research progress in wave Bragg resonance. Advances in Science and Technology of Water Resources 36 (3), 83-87. (in Chinese).

Zheng, Z., Ma, X., Ma, Y., Perlin, M., Dong, G., 2021. Numerical investigation of seismic-induced harbor oscillations. Coastal Engineering 165, 103838.